Zinc and boron co-doped nanotitania with enhanced photocatalytic degradation of Acid Red 6A under visible light irradiation

Ravi Kumar Mulpuri, Siva Rao Tirukkovalluri[*], Manga Raju Imandi, Shaik Abdul Alim and Venkata Divya Lakshmi Kapuganti

Abstract

The present investigation summarizes the synthesis and characterization of zinc and boron co-doped TiO_2 nano catalyst by sol gel method at relatively low temperature and explored the optimum reaction parameters for the degradation of Acid Red 6A (AR 6A) under visible light irradiation. The structural, morphological, surface properties of the synthesized photocatalysts were characterized by X-Ray Diffraction, Scanning Electron Microscopy-Energy Dispersive X-ray Spectroscopy, Transmission Electron Microscopy, Brunauer-Emmett-Teller, UV-Vis-Diffuse Reflectance Spectroscopy, X-ray Photo Electron Spectroscopy and Fourier Transform-Infra Red Spectroscopy. The findings of the characterization results revealed that Zn^{2+} ion was substitutionally doped into TiO_2 lattice by replacing Ti^{4+} ion and a part of the boron substituted the oxygen in TiO_2 lattice and the remaining amount was converted to B_2O_3 due to calcinations at 450 °C. The degradation of AR 6A was achieved at optimum reaction parameters, such as pH = 6 with a catalyst dosage 100 mg L^{-1} for the degradation of 5 mg L^{-1} of dye solution.

Keywords: Zinc and boron co-doped TiO_2, Co-doping, Acid Red 6A, Sol-gel method

Introduction

For the degradation of a wide range of organic dye contaminants from textile and food industry, advanced oxidation process using semiconductors was considered as one of the most promising methods. Mijin et al. [1] reported the use of semiconductors that can be easily controlled with low power consumption. Among all the semiconductors, Titanium dioxide (TiO_2) based photocatalysts were used effectively for the degradation of toxic organic pollutants due to its unique properties like bio-compatibility, low cost, water insolubility, chemical stability and non photocorrosive nature [2]. However, its large band gap energy (3.2 eV) limits its activity in visible light region. To overcome these limitations of TiO_2, many investigators [3–5] developed a promising method to increase the visible light absorption by chemical doping of metal (Bi, Fe, Au, Zn, Cu, Mg, Co, Mn, Ni)] and non-metal (C, S, B, N, P) ions into titania crystal lattice. Further studies of Huang et al. [6–8] have demonstrated

that the metal ion doping into TiO_2 increases separation rate of the electron hole pairs, increases its electrical conductivity and also directly influences the intrinsic properties of the semiconductor, whereas non-metal ion doping reduces the charge recombination rate of photo generated electron-hole pairs. Metal and non-metal co-doped TiO_2 based photocatalysts with more specific surface area and narrow pore size distribution are the promising materials used for various applications in photocatalysis studied by Tan et al. [9]. Others [10, 11] attempted metal and non-metal (Cu & S, Fe & B) co-doping into TiO_2 lattice which resulted in the improved photocatalytic activity by minimizing the band gap, decreasing particle size, increasing the surface area and improved the trapping-to-recombination rate [12]. Among all the transition metals, zinc is more effective dopant for titania, since ionic radii of Zn^{2+} (0.74 A°) is very close to Ti^{4+} (0.75 A°) [13]; thus Ti^{4+} ion can be easily substituted by Zn^{2+} ion into TiO_2 crystal lattice. Doping of zinc into TiO_2 increases the surface area of TiO_2 and facilitates the formation of surface bound OH_3 on the TiO_2 surface [14]. By doping zinc in TiO_2 the band gap

* Correspondence: sivaraoau@gmail.com
Department of Inorganic and Analytical Chemistry, Andhra University, Visakhapatnam 530003, India

energy of TiO_2 is decreased when compared with undoped TiO_2 [15]. Boron doping can effectively inhibit the growth of crystal size [16]. In view of these advantages, it is proposed to synthesize zinc, boron co-doped TiO_2 by eco-friendly single step sol-gel process, which is one of the simple techniques, to control the grain size and produce the porous homogeneous powder. Acid Red (AR) 6A, a model dye pollutant was used to determine the photocatalytic efficiency of the prepared catalysts under visible light irradiation. Acid Red 6A (AR 6A) has been selected based on its toxic effects [17] on skin, kidney, liver, oral cavity and on subcutaneous glands. And also it is highly persistent in environment due to non-biodegradability [18, 19].

Experimental
Materials
Titanium tetra-n-butoxide (E-Merck, Germany), zinc nitrate (E-Merck, Germany), triethyl borate (Sigma Aldrich) were used as precursors for Ti, Zn and B respectively. All the chemicals used were of reagent grade and the solutions prepared in double distilled water without further purification.

Synthesis of zinc, boron co-doped TiO_2
Catalyst samples were prepared by varying different weight percentage of dopants (Zn and B) using sol-gel method. In 150 mL Pyrex glass beaker, titanium tetra-n-butoxide (15 mL) was dissolved in absolute alcohol (30 mL) and stirred for 10 min followed by addition of HNO_3 (2.1 mL) drop wise under continuous stirring for 30 min (Solution I). In another Pyrex glass beaker, absolute alcohol (30 mL), H_2O (4.32 mL), and the dopants, i.e., zinc nitrate and triethyl borate were taken as per the required weight percentages with respect to titanium as shown in the Table 1 (Solution II). At room temperature and under vigorous stirring, the solution II was slowly added to solution I from the burette until the transparent sol was formed, and stirring was continued for 2 h. The sol formed is kept aside for 48 h for aging in dark at

room temperature to obtain gel. The gel was dried in an oven at 100 °C and ground. The catalyst powder was calcined at 450 °C in a muffle furnace for 5 h. The prepared catalysts were labelled as ZBT_1, ZBT_2, ZBT_3, ZBT_4, ZBT_5 and ZBT_6 as presented in Table 1.

Characterization of catalysts
Prepared photocatalysts were characterized by using various instrumental techniques. Ultraviolet-Visible Diffuse Reflectance Spectroscopy (UV-Vis-DRS) spectra were recorded using Shimadzu 3600 UV-Vis-DRS NIR spectrophotometer with an integrating sphere diffuse reflectance. X-Ray Diffraction (XRD) patterns were recorded using ultima IV, RIGAKU model with anode Cu-WL1 λ = 1.5406 nm, nickel filter current 40 mA, voltage 40 kV, 2θ scanning range of 5.000-90.9505°, scan rate of 2 min^{-1}. A PHI quantum ESCA microprobe system, using the ALKα line of a 250 W X-ray tube as a radiation source with the energy of 1253.6 eV, 16 mA × 12.5 kV and working under the pressure lower than 10^{-8} Pa was used to record X-ray Photo Electron Spectroscopy (XPS) spectra. Morphology, chemical composition and particle size of the catalyst particles were determined by Scanning Electron Microscopy (SEM; JSM-6610 LV) equipped with an Energy Dispersive X-ray spectroscopy (EDS) operated at voltage 20 kV and Transmission Electron Microscopy (TEM) (TECNAI FE12) operated at voltage 120 kV. Brunauer-Emmett-Teller (BET) (NOVA 2200 E) system was used to determine pore size, pore volume and surface area of anatase particles from N_2 adsorption-desorption isotherms at 77.3 K. Fourier Transform-Infra Red Spectroscopy (FT-IR) spectrometer (Nicolot Avatar-360) was used to record FT-IR spectra of prepared catalyst. UV-Vis-DRS spectrophotometer (Shimadzu 1601) was used to monitor the degradation percentage of AR 6A dye.

Photocatalytic activity of the Zn and B co-doped TiO_2 nano material
The detailed description of photo-reactor was given elsewhere [20] and photocatalytic procedure was carried out as follows. Required amount of catalyst was added to 90 mL of aqueous solution in a Pyrex glass vessel and stirred the solution in dark for 30 min. Then 10 mL of AR 6A dye (10 mg L^{-1}) was added and continued the stirring for 30 min to achieve the adsorption-desorption equilibrium between catalyst surface and dye molecules. The high pressure metal halide lamp (400 W) with UV filter (Oriel 51472) was used as a visible light source with output 436-546 nm, 35000 lm and placed at a distance 20 cm from the reaction vessel. Running water was circulated around the sample container to filter IR radiation and

Table 1 Name assigned to different weight percentage of TiO_2 co-doped catalysts

Sample No.	Code	Dopants wt%	
		Zn	B
1	ZBT_1	0.75	0.25
2	ZBT_2	1.0	0.25
3	ZBT_3	0.50	0.50
4	ZBT_4	0.25	0.75
5	ZBT_5	0.25	1.0
6	ZBT_6	0.25	0.25
7	Undoped TiO_2	–	–

to keep the reaction mixture at room temperature. The pH of the solution was adjusted before exposed to light illumination by the addition of 0.1 N HCl/0.1 N NaOH to get the required pHs. After the illumination, 5 mL aliquots of samples were withdrawn from the reaction mixture using Millipore syringe (0.45 μm) at different time interval and their concentration was determined using UV-Vis spectrophotometer (Milton Roy Spectronic 1201) at maximum absorbance (λ_{max}) 515 nm. The percentage of degradation of the dye (AR 6A) was calculated by using the following Eq. (1).

$$\% \text{ of AR 6A degradation} = \frac{A_0 - A_t}{A_0} \times 100 \qquad (1)$$

where A_0 is initial absorbance of dye solution before degradation and A_t is absorbance of dye solution at time t.

Results and discussion

XRD

The XRD patterns of undoped and co-doped TiO_2 samples are given in Fig. 1 indicating the formation of less dense anatase phase (JCPDS NO: 21–1272) [21] with corresponding (101) plane of high intensity at 2θ = 25.3°. The other peaks were observed at 2θ of 38.1, 47.9, 75.4 and 83.2° corresponding to (004), (200), (215) and (224) planes, respectively. The less dense anatase phase formation was may be due to more electropositive nature of zinc with loosely held electronic clouds in each TiO_2 matrix as reported by Venkatachalam et al. [22]. There are no characteristic peaks observed for zinc oxides in XRD spectrum in all the co-doped samples, which implies that Zn^{2+} ions are incorporated into the lattice of TiO_2 by substituting Ti^{4+} ion [13], whereas B^{3+} ion
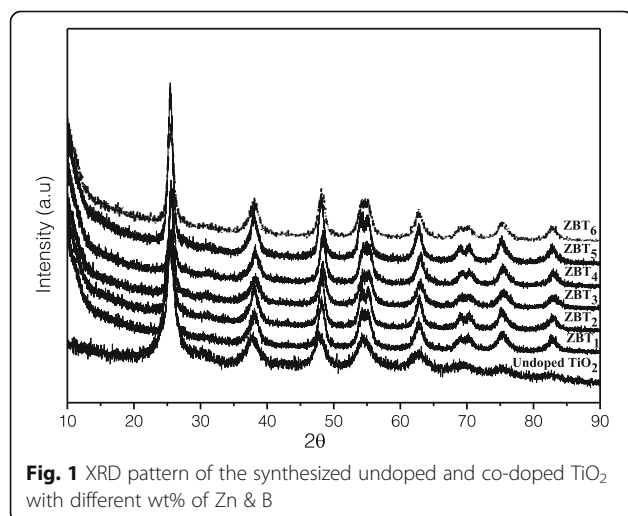

Fig. 1 XRD pattern of the synthesized undoped and co-doped TiO_2 with different wt% of Zn & B

cannot substitute Ti^{4+} ion in the TiO_2 lattice due to large ionic radii difference between Ti^{4+} (61 pm) and B^{3+} (23 pm) ions. On the contrary, a part of the boron ions substitute the oxygen and the remaining small amount of boron ions converted to B_2O_3 at 450 °C calcinations temperature. But in the XRD of all co-doped samples, B_2O_3 peak was not observed, due to decrease in the c-axis parameter of ZBT catalysts and its minute quantity was lower than the detection limit of XRD technique [14]. The average crystallite size of undoped and co-doped TiO_2 samples was determined by Debye-Scherer equation [23] shown in Table 2. Results from the table inferred that the crystallite size of co-doped samples were found to be lesser (ranging from 9.1 to 14.0 nm) than that of undoped TiO_2 (36.5 nm). Among all co-doped TiO_2 samples ZBT_3 (0.50 wt% of Zn & 0.50 wt% of B) exhibits the smallest crystallite size due to inhibition of the crystal growth of TiO_2. The comparative results of undoped TiO_2, zinc & boron single doped TiO_2 and Zn, B co-doped TiO_2 (ZBT_3) crystallite sizes are given in the Table 2.

XPS

The surface chemical composition and electronic states of each constituent elements of the TiO_2 (ZBT_3) were identified as depicted in Fig. 2a-f. The XPS survey spectrum (Fig. 2a) explored the presence of Ti, B, Zn, and O on the surface of ZBT_3 catalyst. The oxidation states of these elements are identified as Ti^{4+}, B^{3+}, Zn^{2+} and O^{2-} based on their binding energies obtained from the magnifying spectra as shown in Fig. 2b-f. Ti^{4+} state was confirmed by the peaks located at 460.1 and 465.7 eV, which correspond to Ti $2p_{3/2}$ and Ti $2p_{1/2}$, respectively [24]. The binding energy peak of boron 1 s appears at 193.5 eV sustained the B^{3+} state. The peaks of Zn $2p_{3/2}$ and Zn $2p_{1/2}$ located at binding energies of 1023.5 and 1045.9 eV, respectively [25], confirmed the presence of Zn^{2+} state in the catalyst. The XPS spectra of O 1 s (Fig. 2d) show two peaks at binding energies of 531.7 and 533.5 eV, which correspond to lattice oxygen (O^{2-}) of TiO_2 and adsorbed H_2O/OH on the surface, respectively [23].

FT-IR

FT-IR spectra of undoped and co-doped TiO_2 (ZBT_3) samples are described in Fig. 3. The peaks at 3400 and 1628 cm^{-1} corresponding to stretching and bending vibrations of H_2O and OH, respectively [26]. Ti-O-Ti stretching frequency band in undoped TiO_2 was observed at 512 cm^{-1} [27, 28] which was shifted to 576 cm^{-1} in the ZBT_3 catalyst. This shift in the frequency of the Ti-O-Ti network is due to the doping of Zn and B ions into TiO_2 lattice. This leads to the distortion in octahedral co-ordination around Ti^{4+} ions by the formation of new interactions Ti-O-Zn and B-O, with
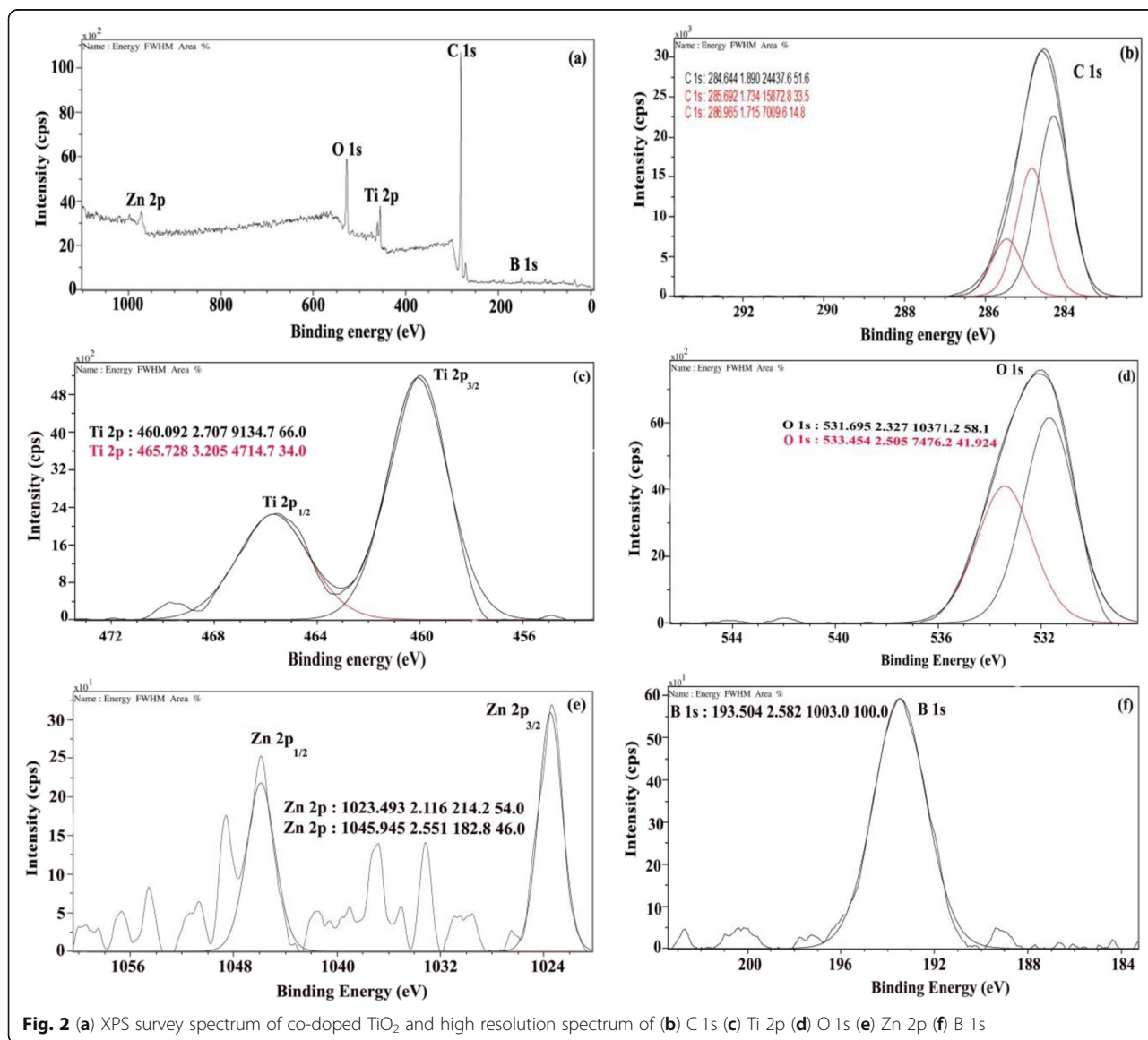
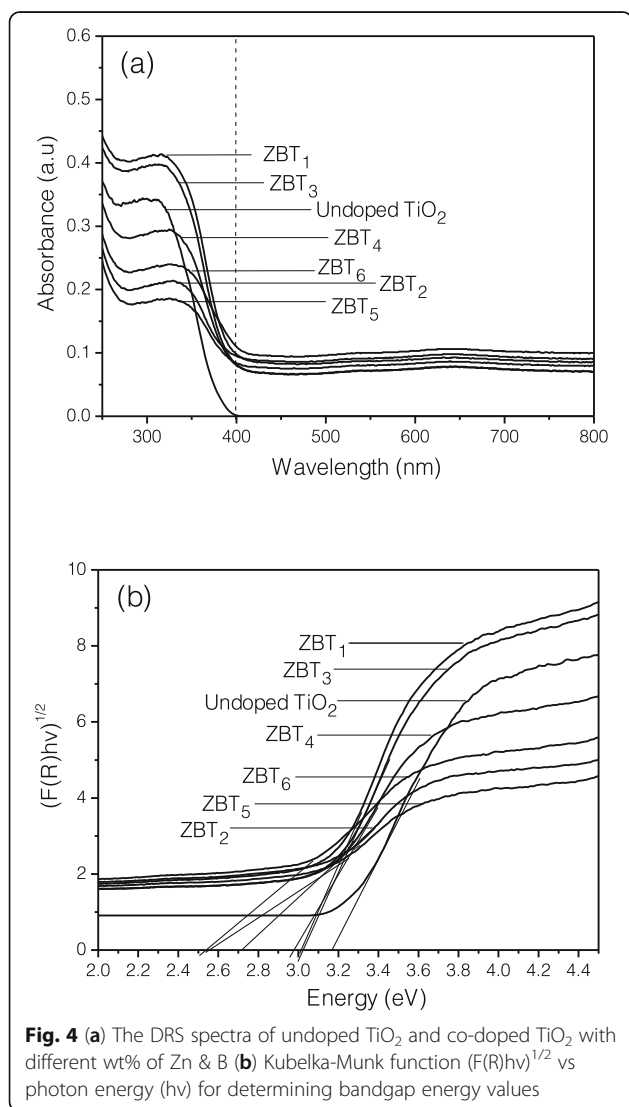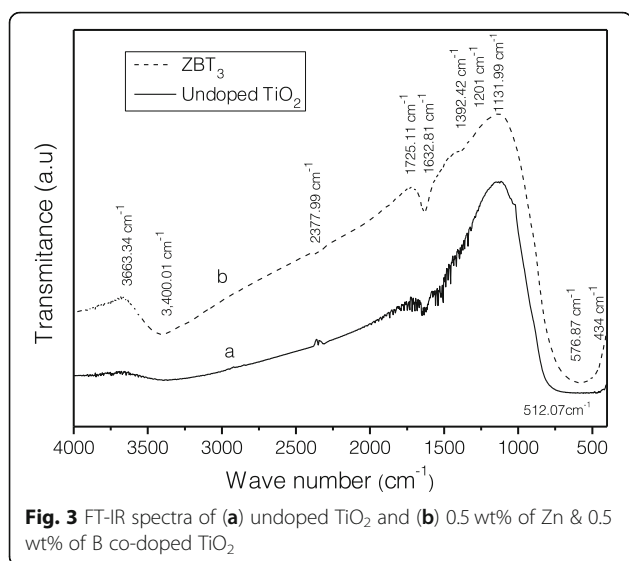**Table 2** Results of band gap (UV-Vis-DRS), crystallite size (XRD), particle size (TEM) and BET surface area

Catalyst	Band gap (eV)	Crystallite size (nm)	Particle size (nm)	Surface area ($m^2 g^{-1}$)
Undoped TiO_2	3.12	36.5	8	47
Zn-TiO_2 (5 mol% Zn) [16]	2.83	14	13	63
B-TiO_2 [24]	2.95	18.5	15	49
Zn,B-TiO_2 (0.50 wt% of Zn & 0.50 wt% of B)	2.49	9.1	5.6	91

stretching vibrations found at 1201 and 434 cm^{-1}, respectively [29]. The asymmetric B-O stretching band was observed at 1392 cm^{-1} [30] due to interstitial doped B^{3+} ion forming the Ti-O-B-O-Ti and substitutional B occupying O sites in a meta stable configuration [31] in the lattice of TiO_2 but because of to low concentration of B and high dispersion, the corresponding peaks were absent in XPS. Hence, FT-IR study confirmed that Zn^{2+} and B^{3+} ions were substitutionally doped into TiO_2 lattice by replacing Ti^{4+} and O^{2-} ions, respectively.

UV-Vis-DRS

The DRS of undoped and co-doped TiO_2 samples are given in Fig. 4a. It is noticed that the co-doped TiO_2 catalysts exhibited extended optical response in visible part of the spectrum. When compared to undoped TiO_2, the

Fig. 2 (**a**) XPS survey spectrum of co-doped TiO_2 and high resolution spectrum of (**b**) C 1s (**c**) Ti 2p (**d**) O 1s (**e**) Zn 2p (**f**) B 1s

Fig. 3 FT-IR spectra of (**a**) undoped TiO_2 and (**b**) 0.5 wt% of Zn & 0.5 wt% of B co-doped TiO_2

Fig. 4 (**a**) The DRS spectra of undoped TiO_2 and co-doped TiO_2 with different wt% of Zn & B (**b**) Kubelka-Munk function $(F(R)h\nu)^{1/2}$ vs photon energy ($h\nu$) for determining bandgap energy values

red shift in co-doped samples indicated the decrease in band gap. This was caused by the extra energy level created above the valance band of TiO_2 by Zn 2p [32] and substitution of B can also narrow the band gap of co-doped TiO_2 [31]. Further it was supported by the calculated band gap energies of the all synthesized catalysts using the Kubelka-Monk formalism and Tauc plot method [13] as shown in Fig. 4b. The undoped TiO_2 exhibited the band gap of 3.12 eV but for the co-doped TiO_2 samples showing the band gap ranging from 2.49 to 2.92 eV. Among all the co-doped samples ZBT_3 exhibiting the lowest band gap energy, i.e., 2.49 eV. The results indicated co-doping of Zn and B made all the catalysts to be visible light active, by which more number of electron-hole pairs is generated by the absorption of visible light and leads to higher photocatalytic activity.

SEM-EDX

The surface morphology and chemical composition of undoped TiO_2 and ZBT_3 catalyst were studied by Field Emission SEM (FESEM) and EDX analyses and the results are shown in Fig. 5a-d. The SEM images of undoped TiO_2 (Fig. 5a) shows smooth and spherical shaped agglomerated particles with uneven size distribution. Compared to undoped TiO_2, ZBT_3 exhibits (Fig. 5b) less agglomerated spherical shaped particles with decreased particle size. From these results it can be inferred that agglomeration and particle sizes were reduced greatly in ZBT_3 by co-doping of Zn and B, which further confirmed by EDX analysis. Compared to undoped TiO_2 (Fig. 5c) the EDX spectrum of ZBT_3 (Fig. 5d) also showed the peaks corresponding to co-doped elements Zn and B. Here the carbon element comes from residual carbon in the testing environment.

TEM

As shown in Fig. 6a and b, the undoped and co-doped TiO_2 nano catalysts are found to have spherical shape. The concentration of the dopants influences the size of the particle [33]. It reveals that the co-doped sample particle sizes are less than that of undoped TiO_2. The select area *electron diffraction* (SAED) pattern of the ZBT_3 shown in Fig. 6c illustrated anatase crystalline phase of TiO_2. From the high-resolution TEM (HRTEM) image shown in the Fig. 6d, the lattice fringes with inter planar distance of 0.32 and 0.29 nm are observed, which corresponds to the (101) and (001) planes of anatase TiO_2, respectively. It indicates a single crystalline structure. The particle size distribution histogram obtained by Guassian fitting method shown in Fig. 6e confirms the average particle size of ZBT_3 as 5.6 nm which
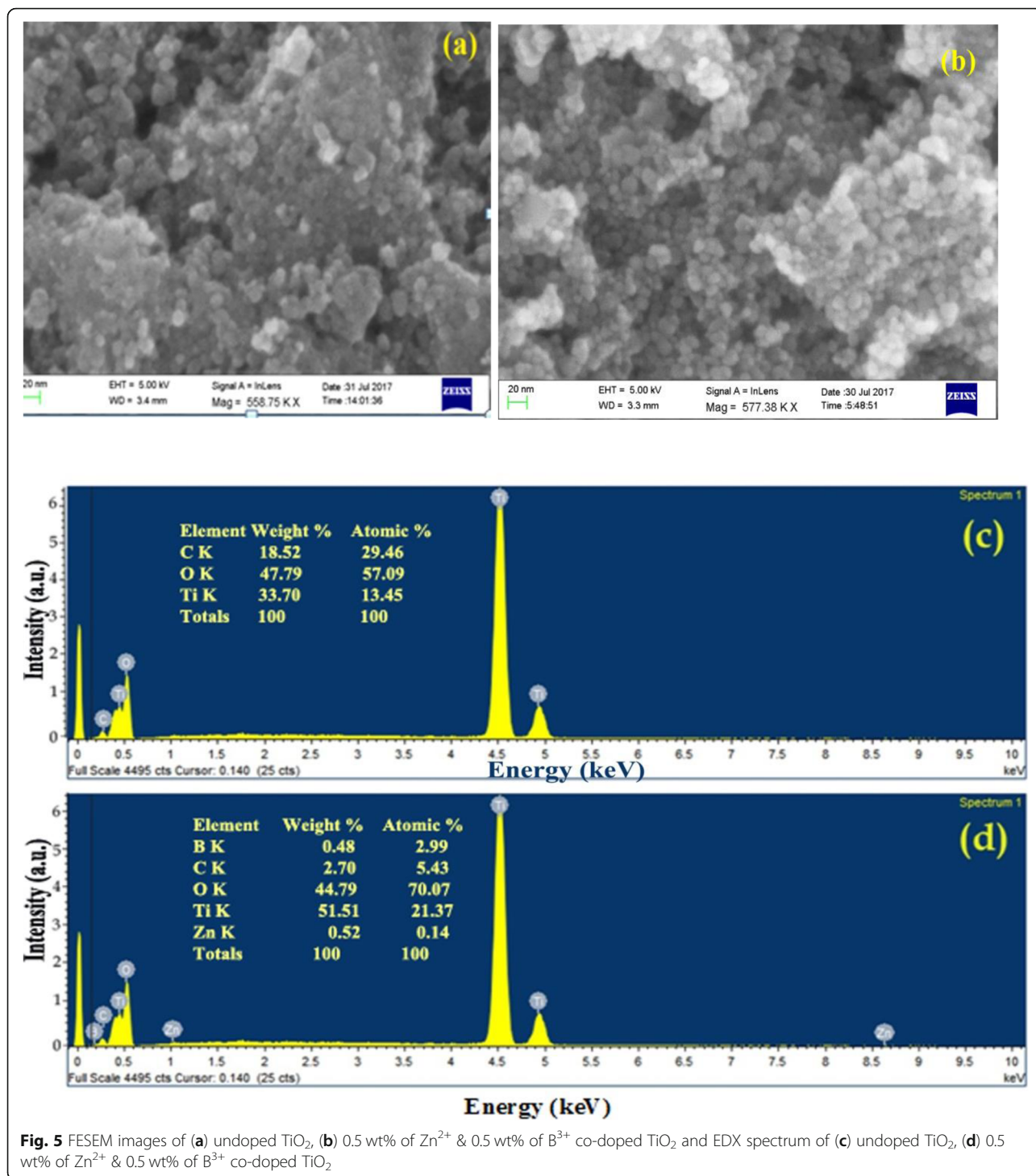
Fig. 5 FESEM images of (**a**) undoped TiO_2, (**b**) 0.5 wt% of Zn^{2+} & 0.5 wt% of B^{3+} co-doped TiO_2 and EDX spectrum of (**c**) undoped TiO_2, (**d**) 0.5 wt% of Zn^{2+} & 0.5 wt% of B^{3+} co-doped TiO_2

exerts the decreased particle size of TiO_2 due to co-doping of Zn and B.

BET surface area

To investigate the specific surface area and porosity characteristics of undoped TiO_2 and co-doped TiO_2 (ZBT_3), N_2 adsorption–desorption isotherms and their corresponding BJH pore size distributions were recorded (Fig. 7a and b). The isotherm (Fig. 7a) shows the type IV pattern with H3 hysteresis loop, implying that the sample has mesoporous nature [34]. This also is confirmed by the corresponding BJH pore size distribution plot (Fig. 7b), where the sharp peaks observed between 2.2 to 8.6 nm represent the
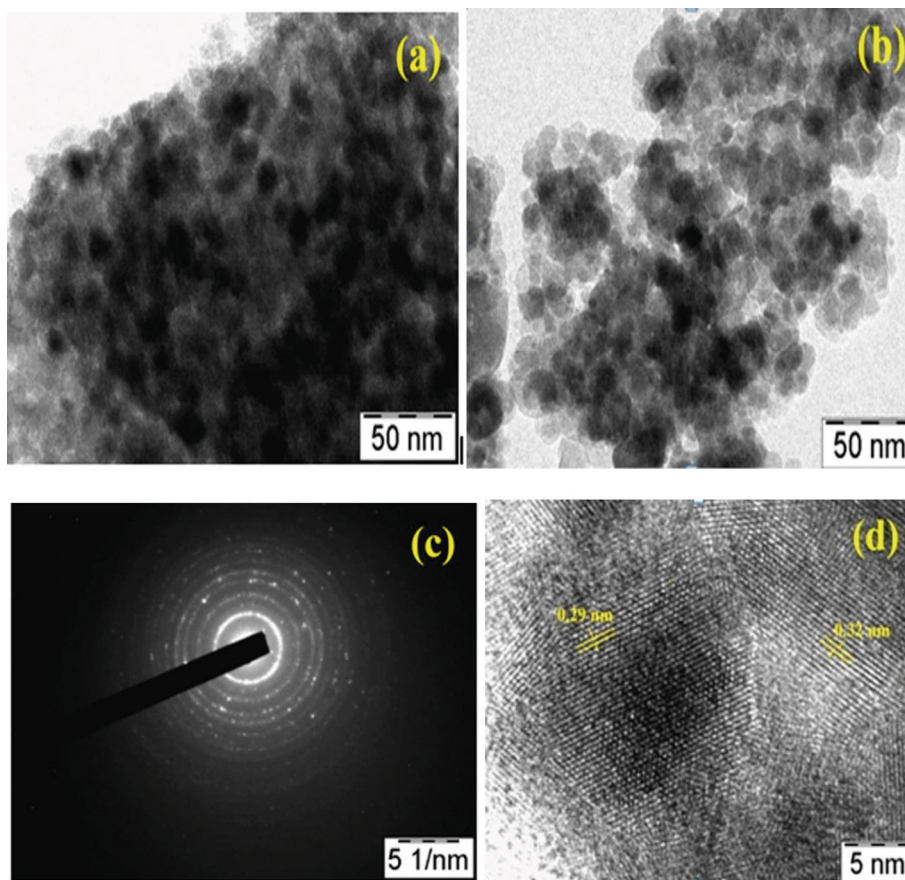
Fig. 6 TEM images of (**a**) undoped TiO_2, (**b**) 0.5 wt% of Zn & 0.5 wt% of B co-doped TiO_2, (**c**) SAED pattern (**d**) HRTEM image and (**e**) particle size distribution of 0.5 wt% of Zn & 0.5 wt% of B co-doped TiO_2

mesopores. Among all the co-doped samples ZBT_3 showed high surface area of 91 $m^2 g^{-1}$. This characteristic feature favours the adsorption of more dye molecules on the catalyst surface which leads to enhance its degradation efficiency.

Evaluation of visible light activity of ZBT_3 on degradation of AR 6A dye

To evaluate the photocatalytic efficiency of synthesized nano catalyst on degradation of AR 6A dye, a series of experiments were conducted under visible light. Initially,
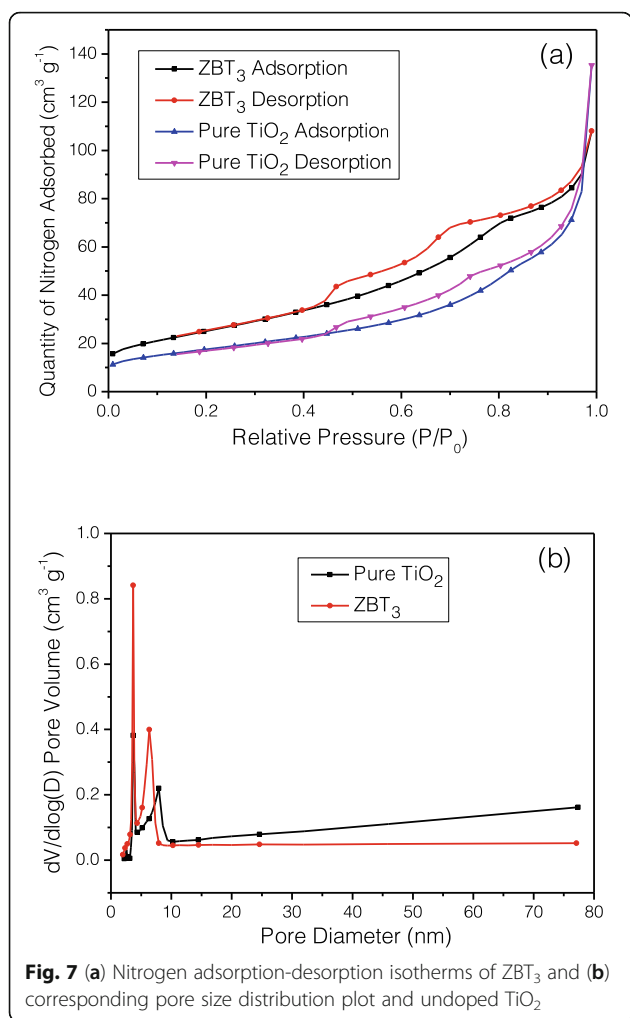
Fig. 7 (**a**) Nitrogen adsorption-desorption isotherms of ZBT_3 and (**b**) corresponding pore size distribution plot and undoped TiO_2

trial experiments were performed by taking only dye solution in the presence and absence of light, where there was no significant degradation observed. Other experiments with dye solution along with synthesized nano catalyst in the presence and absence of light were performed. Here there was a drastic decrease in the absorbance at its λ_{max} 515 nm of the dye in presence of light and small change in the absorbance in absence of light was also observed in the dark, this implies that in the absence of light (dark), there is adsorption of dye molecules on the catalyst surface, and it will cause a slight decrease in the absorbance at λ_{max} 515 nm. This results

indicate that light and catalyst are interdependent on each other. The obtained data are included in the Table 3. To determine the reaction parameter for complete degradation of AR 6A, the following effects were conducted such as i) effect of dopant concentration, ii) pH effect, iii) effect of catalyst loading, and iv) effect of initial dye concentration.

Studies on effect of dopant concentration

To determine the effect of dopant concentrations of co-doped and undoped TiO_2, experiments for co-doped nanocatalysts containing various dopant concentrations were carried out for the photocatalytic degradation of AR 6A with the results presented in Fig. 8a and b and the experimental data presented in the Table 4. All the co-doped samples showed increased photocatalytic rate when compared to undoped TiO_2 under visible light irradiation. This may be attributed to the fact that the co-doping of Zn and B into TiO_2 lattice catalyst becomes visible light active. Among all the co-doped catalysts, ZBT_3 shows highest percentage of degradation due to increased number of charge carriers per particle [35]. At these dopant concentrations, the catalyst particles are having small particle size and high surface area as confirmed by the TEM and BET analysis. Hence, it shows the higher photocatalytic efficiency in degradation of AR 6A. Further increasing the concentration of dopants causes the growth in particle size leads to decrease in surface area and less adsorption of dye molecules on the surface of the catalyst, which limited the rate of degradation. In addition increase in metal dopant concentration creates more electron trap centres [36] and reduce the $^•$OH radical [37].

Further increase in metal ion concentrations in TiO_2, i.e., 0.75 wt% of the catalyst results in decreases in the photocatalytic degradation of AR 6A. This doping of Zn^{2+} ion in TiO_2 lattice minimizes the electron-hole recombination. However, further increases in dopant concentration are found to be detrimental. This is due to the recombination of the charge carriers which depends on the distance 'r' separating e^-/h^+ pair. The recombination rate increases exponentially with the dopant concentration because

Table 3 Results of the percentage (%) of degradation of dye, dye with nanocatalyst sample

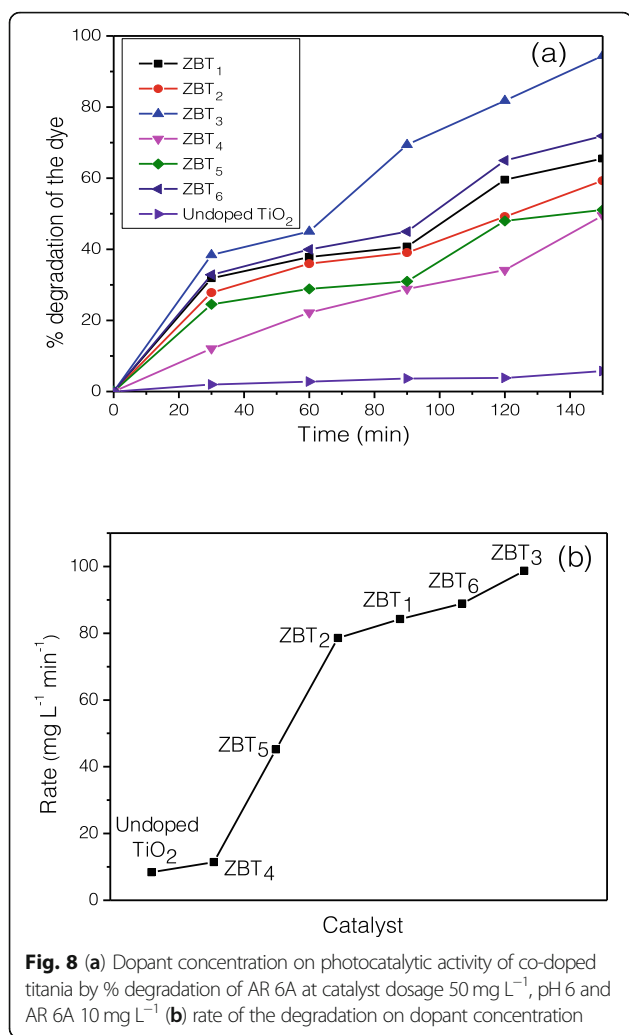| Sample No.	Samples (10 mg L^{-1})	30 min	60 min	90 min	120 min	180 min
1	Dye/in dark	Negligible	Negligible	Negligible	Negligible	Negligible
2	Dye/in light	Negligible	Negligible	Negligible	Negligible	Negligible
3	Dye + ZBT_3/in dark	Negligible	Negligible	Negligible	Negligible	Negligible
4	Dye + ZBT_3/in light	38	45	69	81	94
5	undoped TiO_2	11	19	28	32	34

Fig. 8 (a) Dopant concentration on photocatalytic activity of co-doped titania by % degradation of AR 6A at catalyst dosage 50 mg L^{-1}, pH 6 and AR 6A 10 mg L^{-1} (**b**) rate of the degradation on dopant concentration

Table 4 Effect of dopants concentration on degradation of AR 6A under stimulated visible light irradiation, AR 6A = 10 mg L^{-1}, pH = 6 and catalyst dosage 50 mg L^{-1}

Sample No.	Synthesized catalyst	% degradation of AR 6A dye					Rate (mg L^{-1} min^{-1})
		30 min	60 min	90 min	120 min	150 min	
1	undoped TiO$_2$	2	3	4	4	6	0.08
2	ZBT$_1$	32	38	41	60	66	1.48
3	ZBT$_2$	28	36	39	49	59	1.20
4	ZBT$_3$	38	45	69	82	84	1.51
5	ZBT$_4$	12	22	29	34	49	1.12
6	ZBT$_5$	24	29	38	48	51	1.12
7	ZBT$_6$	33	40	45	65	72	1.53

the average distance between trap sites decreases with increasing the number of dopants. Therefore 0.5 wt% of the Zn^{2+} ion and 0.5 wt% of boron were considered to be an optimal dopant concentration and further photocatalytic experimental effects were carried with ZBT$_3$ catalyst.

Studies on effect of pH

According to Chen [38], the rate of photocatalytic performance of the catalyst can be greatly influenced by pH of the reaction mixture. Experiments were performed by varying the pH from 2 to 8 by keeping the other parameters constant to perceive the pH effect. The experimental data are presented in the Table 5 and the results are shown in Fig. 9a and b, the results indicated that maximum rate was achieved at pH 6 where the surface of TiO$_2$ acquires more positive charge, which facilitate the adsorption of more negatively charged AR 6A dye molecules, consequently it leads to high percentage of degradation. Below the pH 6 the degradation was decreased due to the capturing of photogenerated electrons by the increased number of H$^+$ ions. When the pH increases to basic medium (pH > 7), the catalyst surface changes to negative charge and causes electrostatic repulsion with the similarly charged dye molecules resulting in decreasing rate of degradation [39].

Studies on effect of catalyst loading

Studies on the effect of catalyst loading on degradation of AR 6A is shown in Fig. 10a and b. Experimental data are presented in the Table 6. Various catalyst loadings of 25, 50, 100, 150 mg L^{-1} were added to 100 mL of solution containing 5 mg L^{-1} of dye at pH 6 to investigate the rate of degradation. It is noticed that the rate was increased linearly up to catalyst loading of 100 mg L^{-1} and then decreased on further loading. The decrease can be explained by the turbidity and agglomeration of the catalyst particles, which restricts the penetration of light necessary for the activation of catalyst particles [40], and also collisions between active and ground state catalyst particles results in deactivation of the catalyst particles. Hence, 100 mg L^{-1} of catalyst was found to be the optimum loading.
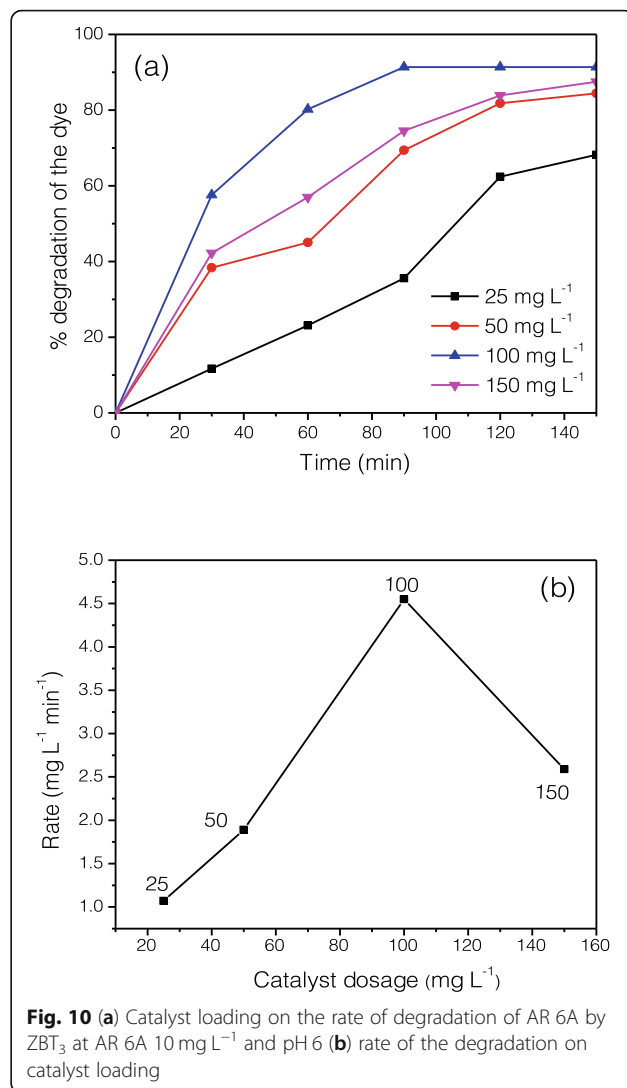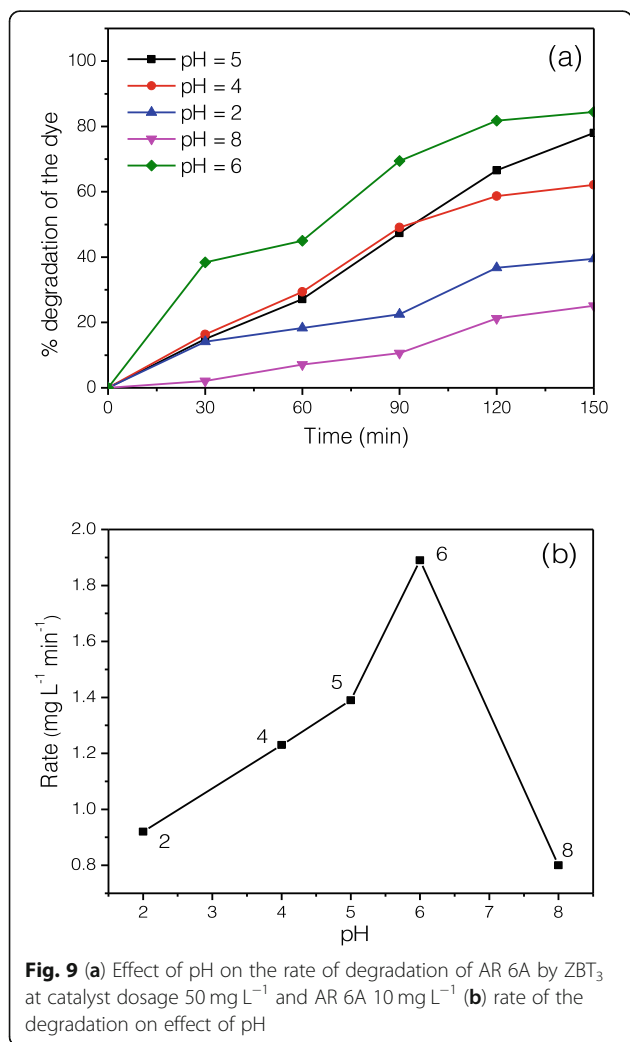
Studies on effect of initial concentration of dye

Different concentrations of AR 6A dye from 2 to 20 mg L^{-1} were used at optimum catalyst (ZBT$_3$) loading of 100 mg L^{-1} and pH 6 to investigate the effect of initial concentration of dye on dye degradation. From Fig. 11a and b, it is observed that the rate of degradation of AR dye is the maximum at 5 mg L^{-1}. Experimental data are included in the Table 7. At higher

Table 5 Effect of pH on the rate of degradation of AR 6A by ZBT$_3$ at catalyst dosage 50 mg L^{-1} and AR 6A 10 mg L^{-1}

pH of the solution	Percentage (%) degradation of AR 6A dye					Rate (mg L^{-1} min^{-1})
	30 min	60 min	90 min	120 min	150 min	
2	14	18	22	37	39	0.92
4	16	29	49	59	62	1.23
5	15	27	47	67	78	1.39
6	38	45	69	82	84	1.89
8	2	7	10	21	25	0.80

concentrations of dye, the rate was decreased due to the deactivation of catalyst particles by the blanket effect. Therefore, the optimum initial dye concentration was found to be 5 mg L^{-1} and also it is not possible to produce corresponding $^{\bullet}$OH radicals to counteract the increased number of dye molecules as the catalyst dosage was fixed.

Fig. 9 (**a**) Effect of pH on the rate of degradation of AR 6A by ZBT$_3$ at catalyst dosage 50 mg L^{-1} and AR 6A 10 mg L^{-1} (**b**) rate of the degradation on effect of pH

Fig. 10 (**a**) Catalyst loading on the rate of degradation of AR 6A by ZBT$_3$ at AR 6A 10 mg L^{-1} and pH 6 (**b**) rate of the degradation on catalyst loading

Conclusions

Zn and B co-doped TiO$_2$ nano catalysts synthesized by sol-gel method exhibit small particle size, less band gap energy and high surface area. In Zn and B co-doped TiO$_2$, Zn significantly influenced the extension of optical absorption towards the visible light region, whereas doping of boron restricted the

Table 6 Effect of catalyst loading on the rate of degradation of AR 6A by ZBT$_3$ at AR 6A 10 mg L^{-1} and pH = 6

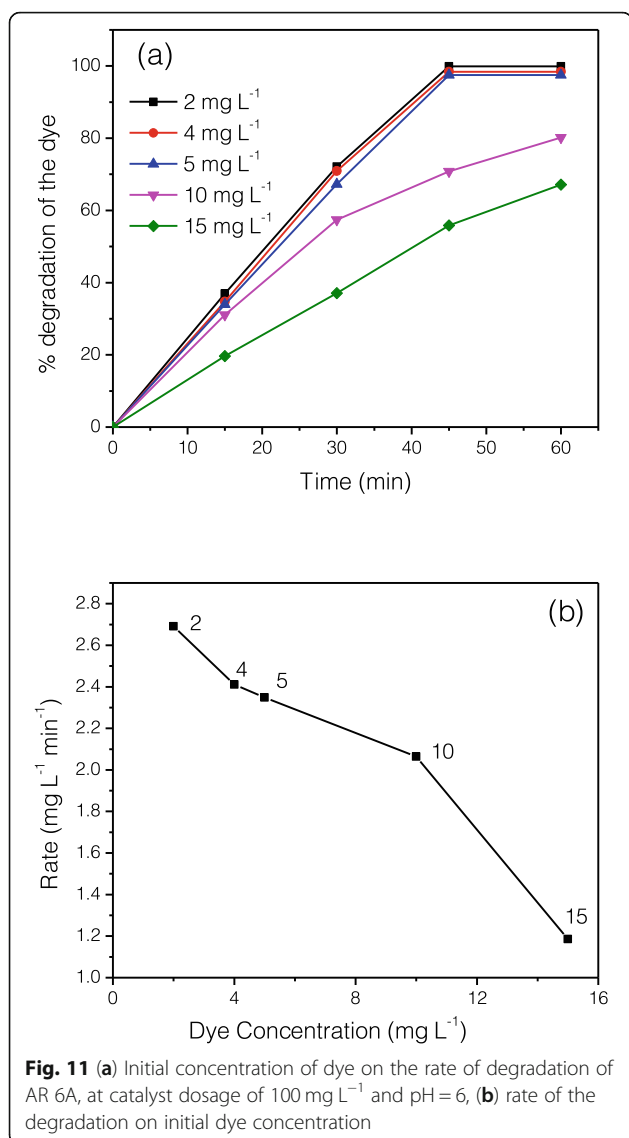| Catalyst dosage (mg L^{-1})	Percentage (%) degradation of AR 6A dye					Rate (mg L^{-1} min^{-1})
	30 min	60 min	90 min	120 min	150 min	
25	12	23	36	62	68	1.07
50	38	45	69	82	84	1.88
100	58	80	91	91	91	4.51
150	42	57	74	84	87	2.60

Fig. 11 (**a**) Initial concentration of dye on the rate of degradation of AR 6A, at catalyst dosage of 100 mg L^{-1} and pH = 6, (**b**) rate of the degradation on initial dye concentration

charge recombination and acted as charge carrier during the degradation process. Compared to other nanocatalysts, ZBT$_3$ (0.50 wt% of Zn and 0.50 wt% of B) co-doped TiO$_2$ showed high photocatalytic activity under visible light irradiation. Finally, AR 6A (5 mg L^{-1}), a model dye pollutant was degraded successfully by 100 mg L^{-1} co-doped catalyst (ZBT$_3$) at pH 6.

Authors' contributions
RKM, SRT and SAA carried out the synthesis and characterization of zinc and boron co-doped nanotitania. MRI and VDLK carried out the photocatalytic degradation experiments of Acid Red 6A under visible light irradiation. All authors read and approved the final manuscript.

Competing interests
The authors declare that they have no competing interests.

References
1. Mijin D, Savic M, Snezana P, Smijanic A, Glavaski O, Jovanovic M, et al. A study of the photocatalytic degradation of metamitron in ZnO water suspensions. Desalination. 2009;249:286–92.
2. Di Paola A, Cufalo G, Addamo M, Bellardita M, Campostrini R, Ischia M, et al. Photocatalytic activity of nanocrystalline TiO$_2$ (brookite, rutile and brookite-based) powders prepared by thermohydrolysis of TiCl$_4$ in aqueous chloride solutions. Colloid Surface A. 2008;317:366–76.
3. Choi WY, Termin A, Hoffmann MR. The role of metal ion dopants in quantum-sized TiO$_2$: correlation between photoreactivity and charge carrier recombination dynamics. J Phys Chem-US. 1994;98:13669–79.
4. Liu X, Liu ZQ, Zheng J, Yan X, Li DD, Chen S, et al. Characteristics of N-doped TiO$_2$ nanotube arrays by N$_2$-plasma for visible light-driven photocatalysis. J Alloy Compd. 2011;509:9970–6.
5. Ohno T, Akiyoshi M, Umebayashi T, Asai K, Mitsui T, Matsumura M. Preparation of S-doped TiO$_2$ photocatalysts and their photocatalytic activities under visible light. Appl Catal A-Gen. 2004;265:115–21.
6. Huang HW, Tu SC, Zeng C, Zhang TR, Reshak AH, Zhang YH. Macroscopic polarization enhancement promoting photo- and piezoelectric-induced charge separation and molecular oxygen activation. Angew Chem Int Edit. 2017;56:11860–4.
7. Huang HW, Li XW, Wang JJ, Dong F, Chu PK, Zhang TR, et al. Anionic group self-doping as a promising strategy: band-gap engineering and multi-functional applications of high-performance CO$_3{}^{2-}$-doped Bi$_2$O$_2$CO$_3$. ACS Catal. 2015;5:4094–103.
8. Huang HW, Xiao K, Yu SX, Dong F, Zhang TR, Zhang YH. Iodide surface decoration: a facile and efficacious approach to modulating the band energy level of semiconductors for high-performance visible-light photocatalysis. Chem Commun. 2016;52:354–7.
9. Tan YN, Wong CL, Mohamed AR. An overview on the photocatalytic activity of nano-doped-TiO$_2$ in the degradation of organic pollutants. ISRN Mater Sci. 2011;2011:261219.
10. Zhang JL, Wu YM, Xing MY, Leghari SAK, Sajjad S. Development of modified N doped TiO$_2$ photocatalyst with metals, nonmetals and metal oxides. Energy Environ Sci. 2010;3:715–26.
11. Huang HW, Liu K, Chen K, Zhang YL, Zhang YH, Wang SC. Ce and F comodification on the crystal structure and enhanced photocatalytic activity of Bi$_2$WO$_6$ photocatalyst under visible light irradiation. J Phys Chem C. 2014;118:14379–87.
12. Khan R, Kim SW, Kim TJ, Nam CM. Comparative study of the photocatalytic performance of boron-iron co-doped and boron-doped TiO$_2$ nanoparticles. Mater Chem Phys. 2008;112:167–72.
13. Hamadanian M, Reisi-Vanani A, Majedi A. Synthesis, characterization and effect of calcination temperature on phase transformation and photocatalytic activity of Cu,S-codoped TiO$_2$ nanoparticles. Appl Surf Sci. 2010;256:1837–44.
14. Wu YM, Zhang JL, Xiao L, Chen F. Properties of carbon and iron modified TiO$_2$ photocatalyst synthesized at low temperature and photodegradation of acid orange 7 under visible light. Appl Surf Sci. 2010;256:4260–8.

Table 7 Effect of the initial concentration of dye on the rate of degradation of AR 6A, at catalyst dosage of 100 mg L^{-1} and pH = 6

Dye concentration (mg L^{-1})	Percentage (%) degradation of AR 6A dye				Rate (mg L^{-1} min^{-1})
	15 min	30 min	45 min	60 min	
2	37	72	99	99	2.69
4	35	70	98	98	2.41
5	34	67	97	97	2.34
10	31	57	76	80	2.06
15	20	37	56	67	1.18

15. Devi LG, Murthy BN, Kumar SG. Photocatalytic activity of TiO_2 doped with Zn^{2+} and V^{5+} transition metal ions: influence of crystallite size and dopant electronic configuration on photocatalytic activity. Mater Sci Eng B-Adv. 2010;166:1–6.

16. Aware DV, Jadhav SS. Synthesis, characterization and photocatalytic applications of Zn-doped TiO_2 nanoparticles by sol-gel method. Appl Nanosci. 2016;6:965–72.

17. Putz AM, Wang KZ, Len A, Plocek J, Bezdicka P, Kopitsa GP, et al. Mesoporous silica obtained with methyltriethoxysilane as co-precursor in alkaline medium. Appl Surf Sci. 2017;424:275–81.

18. Wong YX, Yu J. Laccase-catalyzed decolorization of synthetic dyes. Water Res. 1999;33:3512–20.

19. Feng JW, Sun YB, Zheng Z, Zhang JB, Li S, Tian YC. Treatment of tannery wastewater by electrocoagulation. J Environ Sci. 2007;19:1409–15.

20. Chekuri RD, Tirukkovalluri SR. Synthesis of cobalt doped titania nano material assisted by gemini surfactant: characterization and application in degradation of Acid Red under visible light irradiation. S Afr J Chem Eng. 2017;24:183–95.

21. Wu JCS, Chen CH. A visible-light response vanadium-doped titania nanocatalyst by sol-gel method. J Photoch Photobio A. 2004;163:509–15.

22. Venkatachalam N, Palanichamy M, Murugesan V. Sol-gel preparation and characterization of alkaline earth metal doped nano TiO_2: efficient photocatalytic degradation of 4-chlorophenol. J Mol Catal A-Chem. 2007;273:177–85.

23. Meshesha DS, Matangi RC, Tirukkovalluri SR, Bojja S. Synthesis and characterization of Ba^{2+} and Zr^{4+} co-doped titania nanomaterial which in turn used as an efficient photocatalyst for the degradation of rhodamine-B in visible light. S Afr J Chem Eng. 2017;23:10–6.

24. Xie JM, Jiang DL, Chen M, Li D, Zhu JJ, Lu XM, et al. Preparation and characterization of monodisperse Ce-doped TiO_2 microspheres with visible light photocatalytic activity. Colloid Surface A. 2010;372:107–14.

25. Zhang HR, Liang Y, Wu XD, Zheng HW. Enhanced photocatalytic activity of (Zn, N)-codoped TiO_2 nanoparticles. Mater Res Bull. 2012;47:2188–92.

26. Singla P, Sharma M, Pandey OP, Singh K. Photocatalytic degradation of azo dyes using Zn-doped and undoped TiO_2 nanoparticles. Appl Phys A-Mater. 2014;116:371–8.

27. Elmorsi TM, Riyad YM, Mohamed ZH, Abd El Bary HM. Decolorization of mordant red 73 azo dye in water using H_2O_2/UV and photo-Fenton treatment. J Hazard Mater. 2010;174:352–8.

28. Sharotri N, Sud D. Ultrasound-assisted synthesis and characterization of visible light responsive nitrogen-doped TiO_2 nanomaterials for removal of 2-Chlorophenol. Desalin Water Treat. 2016;57:8776–88.

29. Li YX, Ma GF, Peng SQ, Lu GX, Li SB. Boron and nitrogen co-doped titania with enhanced visible-light photocatalytic activity for hydrogen evolution. Appl Surf Sci. 2008;254:6831–6.

30. Bezerra PCS, Cavalcante RP, Garcia A, Wender H, Martines MAU, Casagrande GA, et al. Synthesis, characterization, and photocatalytic activity of pure and N-, B-, or Ag- doped TiO_2. J Brazil Chem Soc. 2017;28:1788–802.

31. Wang YZ, Wu YS, Yang H, Xue XX, Liu ZH. Doping TiO_2 with boron or/and cerium elements: effects on photocatalytic antimicrobial activity. Vacuum. 2016;131:58–64.

32. Nam SH, Kim TK, Boo JH. Physical property and photo-catalytic activity of sulfur doped TiO_2 catalysts responding to visible light. Catal Today. 2012;185:259–62.

33. Gharibshahi E, Saion E. Influence of dose on particle size and optical properties of colloidal platinum nanoparticles. Int J Mol Sci. 2012;13:14723–41.

34. Sing KSW, Everett DH, Haul RAW, Moscou L, Pierotti RA, Rouquerol J, et al. Reporting physisorption data for gas/solid systems with special reference to the determination of surface area and porosity. Pure Appl Chem. 1985;57:603–19.

35. Kapusuz D, Park J, Ozturk A. Influence of boron and/or zirconium doping on morphology and optical properties of titania. In: Nanocon 2011. Brno; 2011 Sep 21–23.

36. Lachheb H, Puzenat E, Houas A, Ksibi M, Elaloui E, Guillard C, et al. Photocatalytic degradation of various types of dyes (alizarin S, Crocein Orange G, methyl red, Congo red, methylene blue) in water by UV-irradiated titania. Appl Catal B-Environ. 2002;39:75–90.

37. Ooka C, Yoshida H, Horio M, Suzuki K, Hattori T. Adsorptive and photocatalytic performance of TiO_2 pillared montmorillonite in degradation of endocrine disruptors having different hydrophobicity. Appl Catal B-Environ. 2003;41:313–21.

38. Chen CC. Degradation pathways of ethyl violet by photocatalytic reaction with ZnO dispersions. J Mol Catal A Chem. 2007;264:82–92.

39. Kusvuran E, Gulnaz O, Irmak S, Atanur OM, Yavuz HI, Erbatur O. Comparison of several advanced oxidation processes for the decolorization of reactive red 120 azo dye in aqueous solution. J Hazard Mater. 2004;109:85–93.

40. Chiou CH, Juang RS. Photocatalytic degradation of phenol in aqueous solutions by Pr-doped TiO_2 nanoparticles. J Hazard Mater. 2007;149:1–7.

Publisher's Note